SUPPORTING INFORMATION

Mass-Selected FeCo Clusters Embedded in Carbon Matrix as Benchmark Nano-Catalysts

Veronique Dupuis[1], Ghassan Khadra[1], Juan Martín Montejano-Carrizales[2], Florent Tournus[1], Faustino Aguilera-Granja[2,3] and Alexandre Tamion[1].*

[1] Institut Lumière Matière, UMR 5306, Université Lyon 1-CNRS, Université de Lyon, 69622 Villeurbanne, France.

[2] Instituto de Fisica "Manuel Sandoval Vallarta" Universidad Autónoma de San Luis Potosí 78000 San Luis Potosí, Mexico

[3] Centro de Física de Materiales CFM-MPC CSIC-UPV/EHU, Donostia International Physics Center (DIPC), 20018 San Sebastián, Spain.

* Corresponding author : Veronique.Dupuis@univ-lyon1.fr

Table of content

1- Density Funtion Theory (DFT) calculations and geometrical description

i) DFT calculations

Our calculations are based on Density Functional Theory (DFT) within the generalized gradient approximation (GGA) formulated by Perdew-Burke-Ernzerhof (PBE),[1] as implemented in the computational package SIESTA (Spanish Initiative for Electronic Simulations with Thousands of Atoms). [2] SIESTA employs numerical pseudo-atomic orbitals as basis sets to solve the single particle Kohn-Sham equations, while the atomic cores are described by nonlocal norm-conserving Troullier-Martins pseudopotential[3] factorized in the Kleinman-Bylander form.[4] The pseudo-potentials for Fe and Co, were generated using the valence configurations $3d^7$, $4s^1$, and $4p^0$ and $3d^8$, $4s^1$, and $4p^0$, respectively. The s, p and d cut-off radii are 2.00, 2.00, and 2.00 a.u. for Fe and 2.05, 2.05, and 2.05 a.u. for Co. The valence states are described using double-ζ doubly polarized basis sets. Further details about the pseudopotentials and basis sets used, as well as about the pertinent tests, can be found in Refs. [5, 6]

All the cluster calculations were performed using a cubic box (24 Å × 24 Å × 24 Å) large enough such that interactions between the cluster and its replicas in neighboring cells are negligible. We have made several proofs to confirm the independence of the total energy values obtained in our calculations for different box sizes. Only the Γ-point was used for the Brillouin zone integration. We used energy cutoff of 250 Ry to define the real-space grid for the electron density. For the geometric optimization of the atomic structures, we employed the conjugate gradient method [7] as implemented in SIESTA until the interatomic forces are smaller than 0.006 eV/Å. We perform full spin polarization calculations and full relaxation without any constrains in the optimization

ii) Geometrical properties

Rhomboidal dodecahedron (R) is an onion-like structure, consisting of a central site (atom Fe or Co) and a series of layers build by atoms, formed by 14 vertices joined by 24 edges forming 12 rhomboidal faces. The vertices are of two types: type 1, 8 of 3 First Nearest Neighbors (FNN) atoms and type 2, 6 of 4 FNN atoms.

Truncated rhomboidal dodecahedron (T) results from carrying out truncations in the rhomboidal dodecahedron structure. The first truncation is carried out eliminating the 6-vertices type 2, obtaining

---

[1] J.P. Perdew, K. Burke, and M. Ernzerhof, Generalized Gradient Approximation Made Simple, Phys. Rev. Lett. **1996,** 77 3865-3868.

[2] J.M. Soler., E. Artacho, J.D. Gale, A. García, J. Junquera, P. Ordejon, and D. Sánchez-Portal, The SIESTA Method for ab initio Order-N Materials Simulation, J. Phys.: Condens. Matter **2002**, 14, 2745-2779.

[3] N. Troullier, and J.L. Martins, Efficient Pseudopotentials for Plane-Wave Calculations, Phys. Rev. B **1991**, 43, 1993-2006.

[4] L. Kleinman, and D.M. Bilander, Efficacious Form for Model Pseudopotentials, Phys. Rev. Lett. **1982,** 48 1425-1428.

[5] F. Aguilera-Granja, R. C. Longo, L. J. Gallego, and A. Vega, Jour. Chem. Physics **2010,** 132, 184507.

[6] T. Alonso-Lanza, A. Ayuela, and F. Aguilera-Granja, Phys. Chem. Chem. Phys. **2016** 18, 21913–21920

[7] W. H. Press, S. A. Teukolsky, W. T. Vetterling, and B. P. Flannery, Numerical Recipes in Fortran, 2nd edition Cambridge University Press, (Cambridge, **1992**).

square faces; the following truncations result from the elimination of the atoms forming the square faces. The number of truncations depends on the size of the original starting cluster.

In our work, we consider three different sizes for the rhomboidal dodecahedron clusters in the reoptimization process: N=15, 65 and 175. We performed truncations only in N=65 and 175 and reoptimized again to fully relax the system. For N=65 we only consider the first one to get a truncated cluster with 59 atoms, formed for 6-square and 12-hexagonal faces. In the case of N=175 we perform two consecutive truncations, the first in the vertices type 2 and the second on small square faces and in this way we have N=169 and N=145 atoms (both with 6 square and 12 non-regular hexagonal faces), respectively. This can be clearly observed in Fig 1S. Table S1 presents the values obtained for the interatomic distances, magnetic moments per atom as well as the number of holes for the different FeCo cluster sizes in CsCl-B2 phase and depending on the central atom for the two configurations with different central atom (Fe or Co).

Table S1 - Interatomic distances (angstroms), magnetic moments (μ_B) and number of holes (e) obtained for FeCo CsCl-B2 phase clusters with different sizes depending on the central atom (see figure S1)

Number of atoms	Central atom	Fe-Fe	Co-Co	Fe-Co	μ_{Fe}	μ_{Co}	μ_{avg}	h_{Fe}	h_{Co}
15(R)	Fe	2.738	2.839	2.416	3.325	2.092	2.481	3.244	2.132
	Co	2.896	2.666	2.414	3.472	2.168	2.594	3.286	2.122
59(T)	Fe	2.899	2.789	2.452	3.059	1.915	2.405	3.232	2.134
	Co	2.882	2.799	2.474	3.149	1.787	2.496	3.247	2.118
65(R)	Fe	2.895	2.787	2.460	3.028	1.753	2.414	3.224	2.102
	Co	2.889	2.800	2.467	3.024	1.764	2.405	3.229	2.108
145(T)	Fe	2.880	2.846	2.478	3.102	1.759	2.507	3.259	2.129
	Co	2.897	2.829	2.468	2.906	1.806	2.316	3.207	2.130
169(T)	Fe	2.892	2.812	2.473	2.924	1.716	2.340	3.218	2.111
	Co	2.883	2.818	2.474	2.956	1.671	2.389	3.225	2.111
175(R)	Fe	2.890	2.808	2.470	2.919	1.672	2.292	3.217	2.108
	Co	2.895	2.816	2.472	2.928	1.670	2.303	3.222	2.105
Bulk FeCo	- -	2.900	2.900	2.510	2.880	1.690	2.290	3.260	2.170

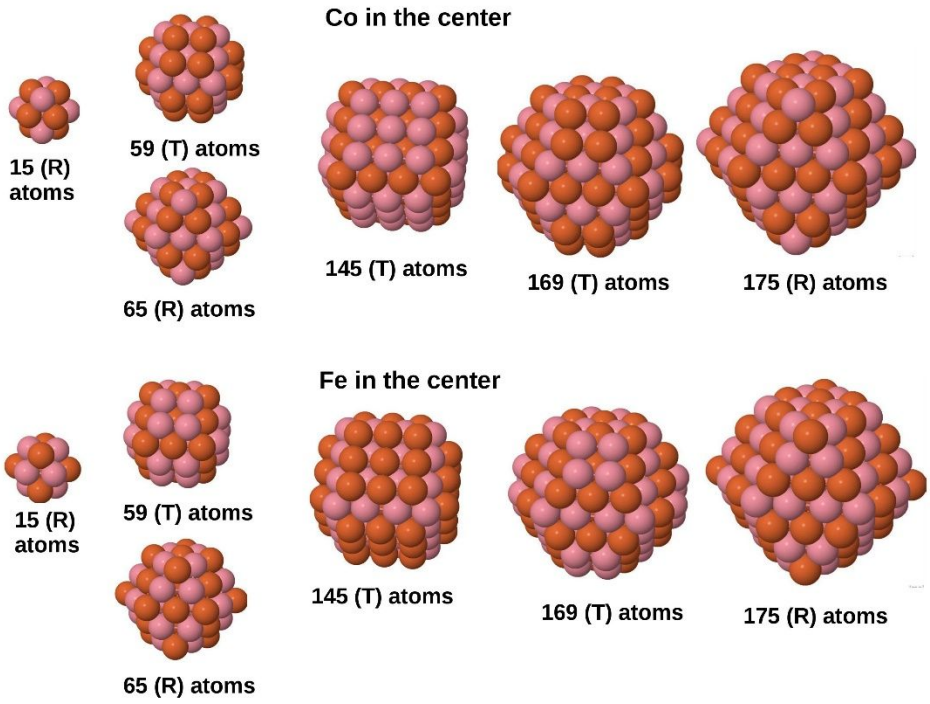

Figure S1 - Schematic representation for FeCo clusters in the CsCl-B2 like-phase for different sizes (N), having different central atoms Co in the upper panel and Fe in the lower. The R stand for those clusters with rhombic dodecahedron shape (N= 15, 65 and 175 atoms), and T stand for truncations made to the dodecahedron one (N= 59, 145 and 169 atoms).

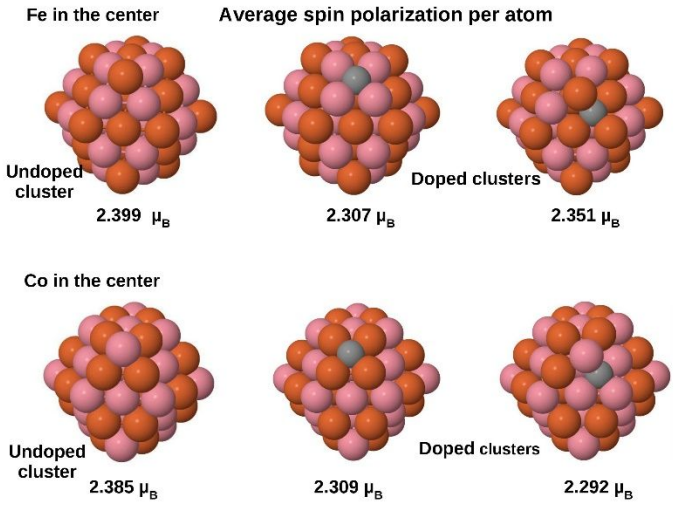

Figure S2 - Schematic representation of B2-FeCo clusters for N=65, including one carbon impurity at different sites with the corresponding average magnetic moments from DFT-calculations.

2- TEM and HRTEM observations on pure and mixed clusters

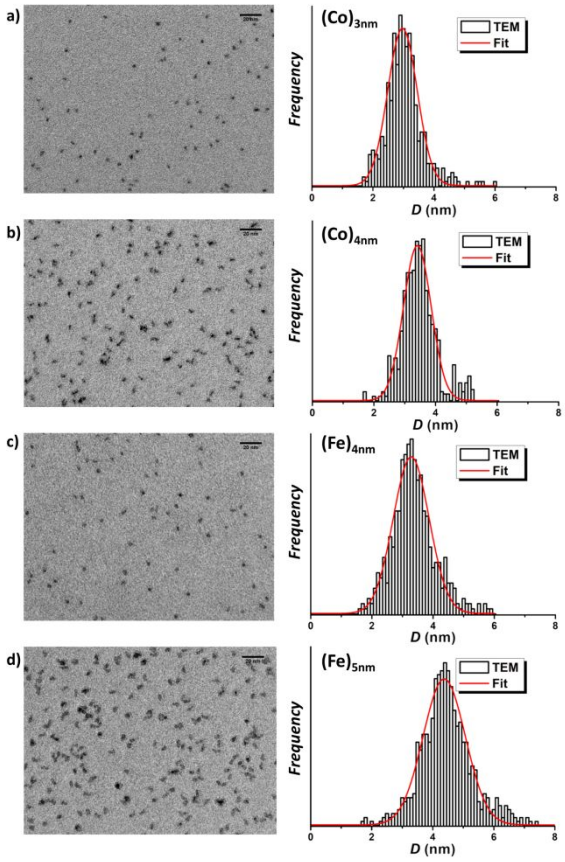

Figure S3 - TEM images for as-prepared mass-selected Co (a, b) and Fe (c, d) nanoclusters and their corresponding size histogram (with Gaussian fit in red continuous line).

Table S2 - Mean diameter and dispersion of mass-selected Co, Fe and FeCo as-prepared nanoparticles. In addition, sphericity values are reported from the ratio of the major to minor axis of the ellipsoidal fit by using a lognormal distribution.

Sample	D_m (nm)	ω	Sphericity	$\omega_{sphericity}$
$(Co)_{3nm}$	2.8 ± 0.2	0.16 ± 0.03	1.41 ± 0.1	0.21 ± 0.03
$(Co)_{4nm}$	3.4 ± 0.2	0.13 ± 0.03	1.63 ± 0.1	0.27 ± 0.04
$(Fe)_{4nm}$	3.3 ± 0.2	0.18 ± 0.03	1.43 ± 0.1	0.22 ± 0.03
$(Fe)_{5nm}$	4.4 ± 0.2	0.16 ± 0.03	1.59 ± 0.1	0.25 ± 0.04
$(FeCo)_{3nm}$	3.7 ± 0.2	0.13 ± 0.03	1.37 ± 0.1	0.16 ± 0.03
$(FeCo)_{4nm}$	4.3 ± 0.2	0.12 ± 0.03	1.47 ± 0.1	0.24 ± 0.04
$(FeCo)_{6nm}$	6.1 ± 0.2	0.1 ± 0.03	1.65 ± 0.1	0.24 ± 0.04

High resolution transmission electron microscopy

Conventional HRTEM images were systematically taken for the three main nanoparticle sizes. For the as-prepared samples, it is clear that not all the nanoparticles are well crystallized. After annealing, even if the nanoparticle to background contrast is not very good, a bcc structure is observed especially for the larger nanoparticle sizes (see figure S4). HRTEM images for the different samples exhibit a FFT that correspond to Miller indices of a bcc structure.

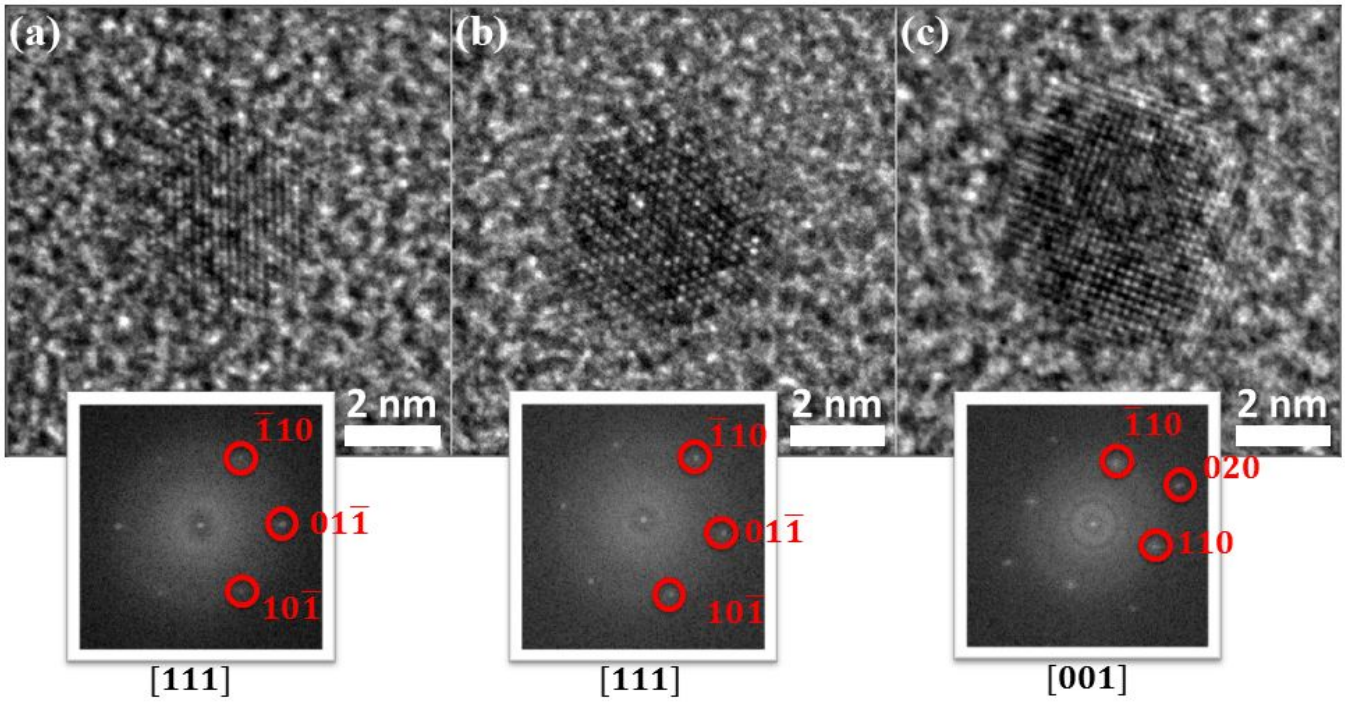

Figure S4 - HRTEM images for annealed $(FeCo)_{3nm}$ (a), $(FeCo)_{4nm}$ (b) and $(FeCo)_{6nm}$ (c) samples along with their corresponding FFT.

3- EXAFS results on as-prepared and annealed Mass-selected pure and bi-metallic FeCo clusters in carbon matrix.

EXAFS on Mass-selected Pure clusters

The Figure S5 shows the thermal evolution of the first nearest-neighbors (NN) radial distribution of pure mass-selected clusters with 4 nm in diameter.

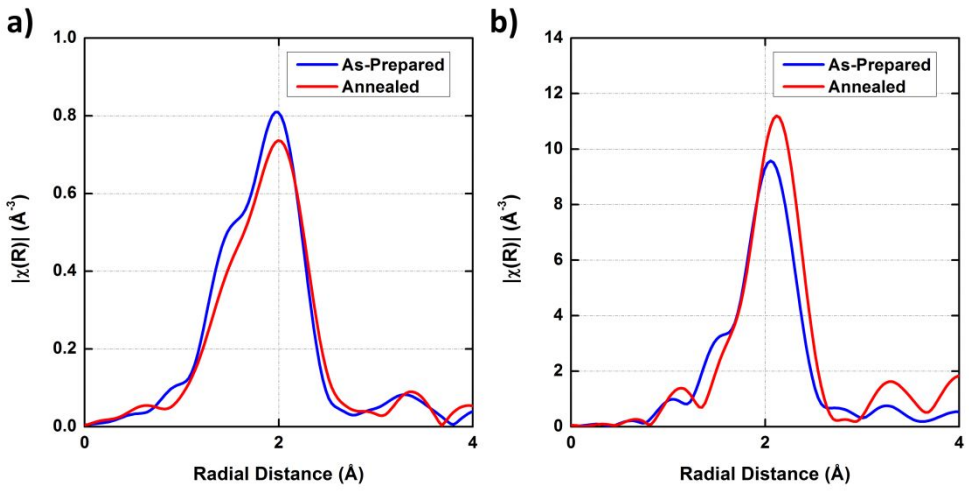

Figure S5 – First NN Radial distributions of EXAFS oscillations for the as-prepared (in blue) and annealed (in red) of pure $(Fe)_{4nm}$ (a) and $(Co)_{4nm}$ (b) samples.

From the above figure, we can clearly see that after annealing the crystal coordination in the Co nanoparticles is enhanced contrary to that in the Fe nanoparticles (Fig. S5a), this is evidenced by the increase in intensity of the principal peak (Fig. S5b). Comparing the shape of the Fe peak with that of iron carbides, it appears that in the as-prepared clusters a Hägg carbide form is present. While after annealing the same carbide is still present but with a reduced crystal order. On the contrary, from qualitative analysis of the radial distribution for Co sample, as well as from quantitatively fitted data, it is clear that after annealing there is a demixing of the cobalt and carbon atoms as already observed in Co particles embedded in carbon matrix from magnetic characterization. [8]

[8] Tamion, A.; Hillenkamp, M.; Hillion, A.; Tournus, F.; Tuaillon-Combes, J.; Boisron, O.; Zafeiratos, S.; Dupuis, V., Demixing in Cobalt Clusters Embedded in a Carbon Matrix Evidenced by Magnetic Measurements, J. Appl. Phys. **2011**, 110, 063904.

EXAFS on Mass-selected Bimetallic FeCo clusters

Figures S6 and S7 show the normalized XAS signal and the radial distribution at the Fe and Co K-edges, respectively, for the **as-prepared** samples for all sizes ($(FeCo)_{3nm}$, $(FeCo)_{4nm}$ and $(FeCo)_{6nm}$).

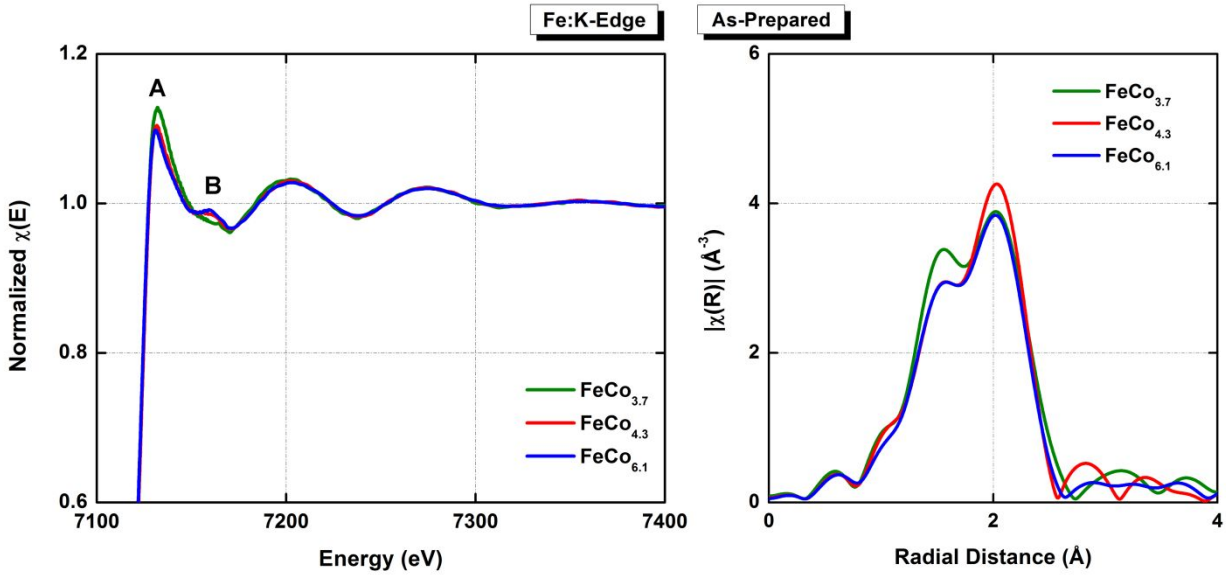

Figure S6 - The normalized XAS signal (left) and NN Radial Distributions of EXAFS oscillations (right) for the as-prepared $(FeCo)_{3nm}$ (green), $(FeCo)_{4nm}$ (red) and $(FeCo)_{6nm}$ samples (blue) at the Fe:K-edge.

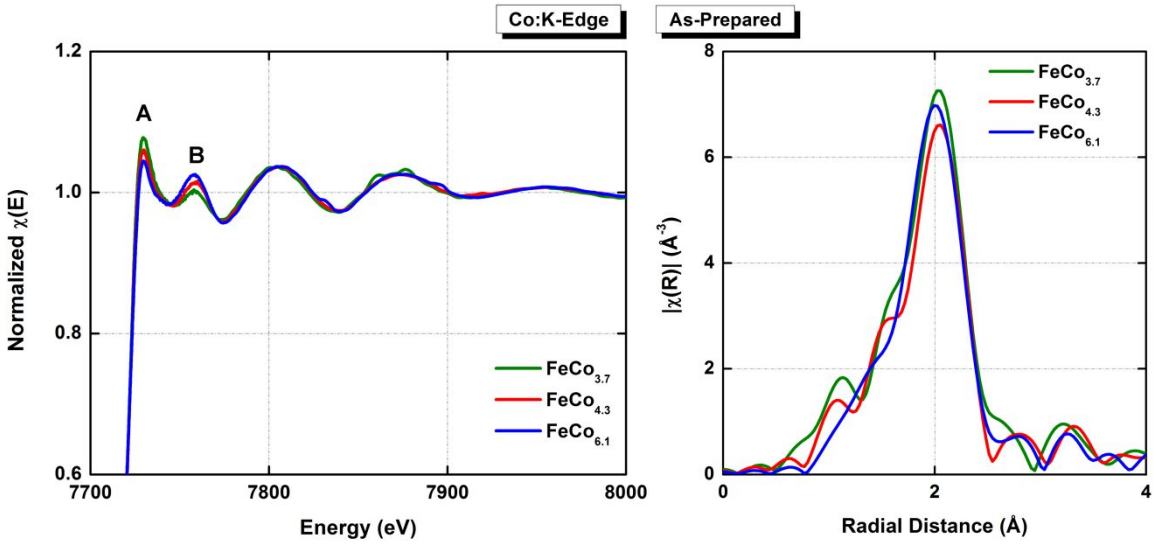

Figure S7- The normalized XAS signal (left) and NN Radial Distributions of EXAFS oscillations (right) for the as-prepared $(FeCo)_{3nm}$ (green), $(FeCo)_{4nm}$ (red) and $(FeCo)_{6nm}$ samples (blue) at the Co:K-edge.

From the normalized XAS signals at both edges, the three nanoparticle sizes exhibit qualitatively the same signature. It is practically impossible to distinguish the difference between the structural information carried by the EXAFS oscillations for the different sizes. Some slight differences can be observed at the X-ray Absorption Near Edge Structure (XANES) except the fact that the smaller the sample size, the higher

white line peak (A) and the smaller first oscillation peak (B). The XANES is often used to determine the valence state of the probed atom[9] (Fe or Co in our case). As the amplitude of the white line peak increases, the carbide signature increases, while the increase of the first oscillation peak indicates a better crystallization (increased ordering). As for the radial distribution, the position of the primary peak is the same for all sizes, with a slight shift for the $(FeCo)_{6nm}$ sample at the Co K-edge. The pre-peak signal is almost the same with some minor deviation from one size to another. The latter is strongly related to the form of the XANES peak and can be used to determine the type of carbide at the iron edge.

Figures S8 and S9 show the normalized XAS signal and the radial distributions of EXAFS oscillations at the Fe and Co K-edges, respectively, for the **annealed samples for all sizes** ($(FeCo)_{3nm}$, $(FeCo)_{4nm}$ and $(FeCo)_{6nm}$).

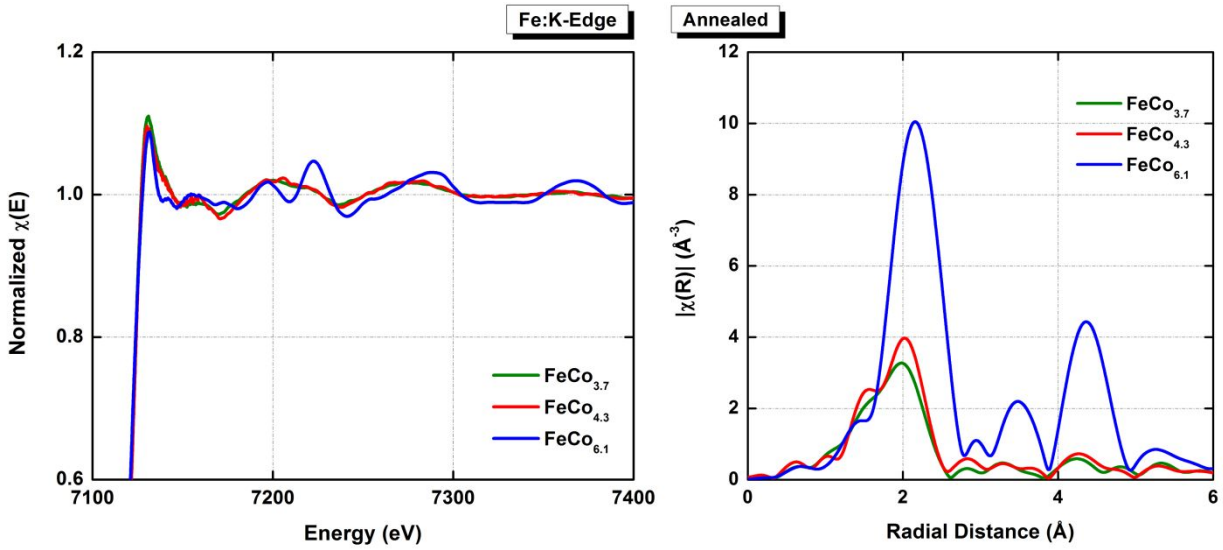

Figures S8 - The normalized XAS signal (left) and Radial Distributions of EXAFS oscillations (right) for the annealed $(FeCo)_{3nm}$ (green), $(FeCo)_{4nm}$ (red) and $(FeCo)_{6nm}$ samples (blue) at the Fe:K-edge.

[9] Bianconi A., Surface X-ray absorption spectroscopy: Surface EXAFS and surface XANES, Applications of Surface Science **1980**, 6, 392-418

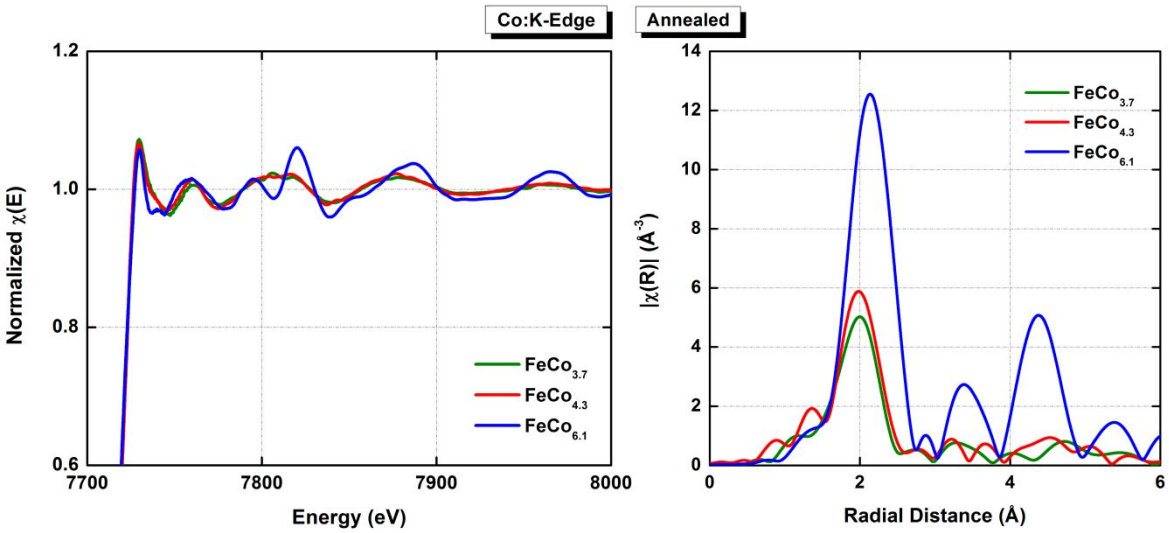

Figures S9- The normalized XAS signal (left) and Radial Distributions of EXAFS oscillations (right) for the annealed $(FeCo)_{3nm}$ (green), $(FeCo)_{4nm}$ (red) and $(FeCo)_{6nm}$ samples (blue) at the Co:K-edge.

For the annealed samples, taking into consideration the $(FeCo)_{3nm}$ and $(FeCo)_{4nm}$ samples, both samples exhibit almost the same EXAFS oscillations with a slight difference of the XANES edge. In analogy with the formation of bct martensite in steels, we obtained an increase in Fe-Fe interatomic distance from 2.46 to 2.51 Å for smaller FeCo size to probably correlate to carbon insertion between iron planes upon annealing.

Comparing the $(FeCo)_{6nm}$ sample with the smaller sizes, from a first glance, a shift of the primary peak is observed at both edges. In addition, oscillations of the radial distribution are clearly visible up to 6Å at both edges (see figure S10) even comparable to the radial distribution of the metallic bcc Fe foil implying that after annealing of the $(FeCo)_{6nm}$ sample, a CsCl-B2 phase FeCo is certainly formed.

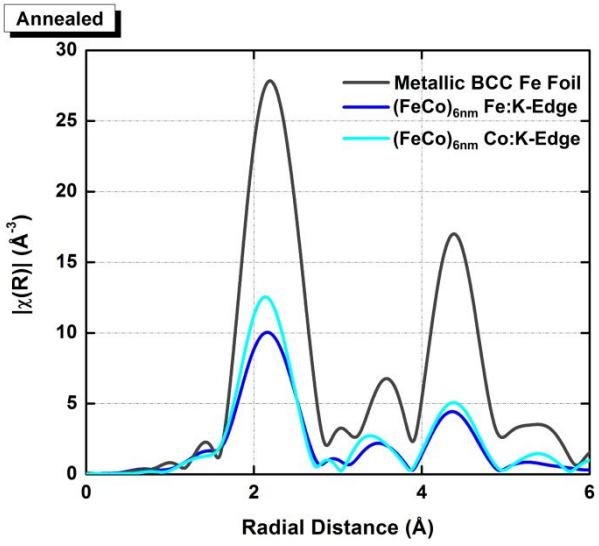

Figure S10 - The radial distributions of EXAFS oscillations for the annealed $(FeCo)_{6nm}$ sample at both Fe and Co K-edges, and for the Fe metallic foil at the Fe K-edge.